 doi:10.20944/preprints202010.0027.v1

Space-Selective Control of Functional Crystals by Femtosecond Laser: a Comparison Between $SrO-TiO_2-SiO_2$ and $Li_2O-Nb_2O_5-SiO_2$ Glasses

Xuan He,[a,b] Qiming Liu,[a*] Matthieu Lancry,[c] Francois Brisset[c] and Bertrand Poumellec[c*]

[a]School of Physics and Technology, Key Laboratory of Artificial Micro- and Nano-structures of Ministry of Education, Wuhan University, Wuhan 430072, P. R. China
[b]The State Key Laboratory of Refractories and Metallurgy, Wuhan University of Science & Technology, Wuhan 430081, P. R. China.
[c]Institut de Chimie Moléculaire et des Matériaux d'Orsay, UMR CNRS-UPS 8182, Bâtiment 410, Université Paris-Saclay, 91405 Orsay Cedex, France
*Corresponding author: bertrand.poumellec@u-psud.fr, qmliu@whu.edu.cn

Abstract: We report on space-selective crystallization of congruent and polar $Sr_2TiSi_2O_8$ crystals in a stoichiometric $SrO-TiO_2-SiO_2$ glass induced by (1030 nm, 300 fs) femtosecond laser irradiation. This allows us to compare with non-congruent laser induced crystallization of polar $LiNbO_3$, in non stoichiometric $Li_2O-Nb_2O_5-SiO_2$ glass and gain information on the mechanism of nanocrystals orientation with the laser polarization that we pointed out previously. Using scanning electron microscopy (SEM), Second-harmonic generation (SHG) and electron backscattered diffraction (EBSD), we studied the laser induced crystallization according to the laser processing parameters (pulse energy, pulse repetition rate, scanning speed). We found 1) a domain where the laser track is filled with crystals not perfectly textured (low energy), 2) a domain where an amorphous volume remain surrounded by a crystallized shell (high energy). This arises from Sr out-diffusion and may gives rise to crystallization of both $SrTiO_3$ and $Sr_2TiSi_2O_8$ phases at low speed. In the one-phase domain (at higher speed), it is found the possibility to elaborate a tube with a perfect fresnoite texture. Significant difference in size and morphology whereas crystallization threshold remains similar are discussed based on glases thermal propeties. Contrarily to $Li_2O-Nb_2O_5-SiO_2$ (LNS) glass, no domain of oriented nanocrystallization controlled by the laser polarization has been found in $SrO-TiO_2-SiO_2$ (STS) glass, which is attributed to the larger crystallization speed in STS glass. No nanogratings have also been found that is likely due to the congruency of the glass.

Keywords: femtosecond laser-induced crystallization; nonlinear crystals; controllable texture; Fresnoite; $Sr_2TiSi_2O_8$; $LiNbO_3$; glass

1. Introduction

Materials functionalized by non-linear crystals exhibiting thus second harmonic generation (SHG) effect have gained rapidly increasing attention due to their widely potential applications in various optical devices over the past two decades [1-3]. Crystallization of glass is one of the easy and low-cost techniques to explore and fabricate new nonlinear optical materials for integrated optic devices. Up to now, several methods, including thermal gradient [4], ultrasonic surface treatment [5] and continuous wave laser irradiation [6] [7], have been proposed to facilitate a controlled crystallization. However, these methods do not allow the control of the crystals' space distribution in volume, whereas it is a key point for the applications in integrated optics. Using cw laser, the light absorption is single photon and usually doping the glass with transition metal or rare earth is necessary ([8]), resulting in surface or shallow modifications.

On the contrary, femtosecond (fs) laser has been proved as a powerful tool to induce three-dimensional crystallization inside glasses. For example in 2000, Miura et al. [9] was one of the first to use a 800 nm fs laser to induce β-BaB_2O_4 crystal inside $47.5BaO-5Al_2O_3-47.5B_2O_3$ glass. Similar results were then reported in $BaO-TiO_2-SiO_2$

 doi:10.20944/preprints202010.0027.v1

glass for inducing Fresnoite crystallization by Dai et al. in 2007 [10] and followed by Stone et al. [11] in 2009 succeeding in direct-writing of ferroelectric single-crystal waveguide of $LaBGeO_5$ from a glass system of the same composition. Then a decade ago, our research group and others have also reported the three-dimensional growth of ferroelectric $LiNbO_3$ crystals [12] that crystallize non-congruently inside Li_2O-Nb_2O_5-SiO_2 glasses [13-15]. $LiNbO_3$ exhibits a strong anisotropy with a non-center symmetric space group R3c. It is polar along the trigonal axis and thus shows the maximum non-linear optical property in this direction. It is a uniaxial crystal but with the largest refractive index being perpendicular to the polar axis [16]. With those properties, we showed it is possible to control the orientation of LiNbO3 nanocrystals appearing at low fs pulse energy, with the laser polarization [17]. This was a breakthrough in material science, whereas at high pulse energy, the crystallization grains are larger with the polar axis directed along the laser scanning direction whatever the laser polarization orientation as it is the case in many publications [7, 8].

One question motivating this work was to see if such possibility to orientate nanocrystals can be found in other glass systems and draw out conclusions about the mechanism and other compounds. As we mention above, Ba-Fresnoite has been already investigated by Dai et al. [10]. A quite recent review reports the various properties of the Fresnoite compounds [18]. Their space group is P4bm, tetragonal and non-center symmetric but even if it exhibits a polar axis and have strong nonlinear optical properties, they are not ferro-electric, but only pyro-electric. In addition Fresnoite is a uniaxial structure with large refractive index perpendicular to the polar axis [19] as for $LiNbO_3$. There are several minerals with Fresnoite structure. The original one is $Ba_2TiSi_2O_8$ but others are $Ba_2Ti(Ge/Si)_2O_8$ or $Sr_2TiSi_2O_8$. They can be obtained from glasses of the same composition in a congruent way contrasting with $LiNbO_3$ from LNS glasses [19]. From these compounds, we chose to test Sr-Fresnoite possessing a remarkable second-order nonlinear coefficient [20]. Its melting temperature is close to the one of $LiNbO_3$ i.e. around 1257 and 1312°C. The glass transition temperature is higher for STS glass by about two hundred °C but the nucleation and growth seem much more efficient [21, 22]

Dai *et al.* [23] used a high repetition rate fs laser to induce $Sr_2TiSi_2O_8$ crystal arbitrarily inside a stoichiometric SrO-TiO_2-SiO_2 glass. This is the usual condition for controlling the average temperature in space and time. Note we made some preliminary investigations in 33.3SrO-16.7TiO_2-50SiO_2 glass already several years ago [24]. Here, we present a much more complete description of the crystallization morphology according to pulse energy, pulse repetition rate and beam scanning speed for looking if nanocrystals elaboration conditions can be found. In this respect, we extend the above works and investigate the influence of laser irradiation parameters on the size, distribution and phase of photo-induced crystals in 40SrO-20TiO_2-40SiO_2 (so called STS glass in the following).

2. Materials and methods

2.1 Preparation of samples

Samples were synthesized by the conventional melt-quenching technique using $SrCO_3$ (99.95%), TiO_2 (99.9%) and SiO_2 (99.9%) as raw materials. Well-mixed reagents were melted in a Pt crucible at 1450°C for roughly 2 hours. Then, the obtained glass melts were poured onto a carbon plate preheated at 200°C. A following annealing was performed at 650°C for 12 hours to release cooling stresses. The glasses were then cut into 10 mm × 10 mm × 1.5 mm-sized pieces and mirror-polished.

2.2 Laser irradiation and material characterization

A Yb-doped fiber amplifying fs laser system was used as light source to irradiate below the glass surface by moving the converging aspheric lens of 150

 doi:10.20944/preprints202010.0027.v1

μm. The main laser parameters are as following: 300 kHz, 300 fs, 1030 nm, and NA=0.6, laser polarization parallel to the scanning direction. The laser inscription experiments and characterizations of samples after irradiation were similar to those given in ref [24].

3. Results

A matrix of static irradiations was firstly performed to determine the crystallization boundary in STS glass. Results are shown in Fig. 1(a) (green dots). For repetition rates below 200kHz, no crystallization is observed. For repetition rates higher than 200 kHz, the minimum average pulse energy is around 1 μJ at 200 kHz (0.2W in average) and reduced to 0.3 μJ at 400 kHz (0.12W). From that, a proper frequency of 300 kHz was used for writing all the lines reported in this paper. We can notice that the average power is comparable with the limit for LNS which was about 0.16W [25].

Fig. 1(b), corresponding to cross-section of two laser traces written at 1.7 μJ pulse energy, with close low scanning speed, shows the now classical tear like shape of the heat affected volume (HAV) with the laser penetrating the material from the top. As usual with fs laser irradiation, we can see several interaction areas (also detectable in Fig. (2)). There is a zone surrounding the internal one and that remained amorphous. It corresponds to the first type of interaction with fs laser : a change of fictive temperature due to the thermal treatment imposed by the scanning beam [26]. Within this shell, the micrograph (in Fig.2) and EBSD analyses (in Fig.3) reveals crystals either in the head of the laser trace cross-section (at 1.5μJ, for various scanning speed) or making up a shell surrounding a non-crystallized volume (at 1.3 μJ) or also a complete crystallized volume surrounded by a thin amorphous shell (at 0.7μJ). The numerous experiments we did, showed that sizes are not strongly dependent on the scanning speed in the limited range investigated here (i.e. smaller than 20 μm/s). On the contrary, when laser power varied from 0.7 up to 1.7 μJ, the interaction volume clearly increased from ~5 to ~50 μm in width and ~18 to ~70 μm in length, respectively.

These observations can be sum-up as following:

1) At low pulse energy, the laser trace is completely crystallized in the Fresnoite system. The c-axis is rather well oriented in the direction of writing when the scanning speed is not too large i.e. below a few μm/s.

2) Increasing the pulse energy, the size of the HAV increases dramatically and a crystallized shell surrounds an amorphous volume. In 3D, this defines an amorphous tube with crystallized walls. Again, the Fresnoite crystals are rather well oriented with c-axis aligned in the direction of beam scanning.

3) Increasing further the pulse energy (1.7μJ at 20 μm/s or 1.5μJ at 10 μm/s), the top of the tube is partially filled (see Fig. 3g).

4) We note that the Fresnoite crystal texture with c-axis in the direction of scanning is deteriorated for large scanning speed (see Fig. 3g).

The <001> pole figures are employed to display the degree of preferred orientation in crystal lines. For 0.7-1.3-1.5 μJ pulse energy, low scanning speed (3 μm/s), most of the crystalline matter is oriented with the polar axis in the scanning direction with a tilted angle for lower pulse energy (Fig. 3 (d)-(f)). When scanning speed is increased, whatever the pulse energy, the crystal texture becomes disordered (see the IPF and pole figures in Fig. 3 (f)-(g)).

5) At high energy but low speed, a $SrTiO_3$ phase appears in the top of the HAV, mixed with Fresnoite and may reach about 50%. of the volume.

Preprints (www.preprints.org) | NOT PEER-REVIEWED | Posted: 1 October 2020 doi:10.20944/preprints202010.0027.v1

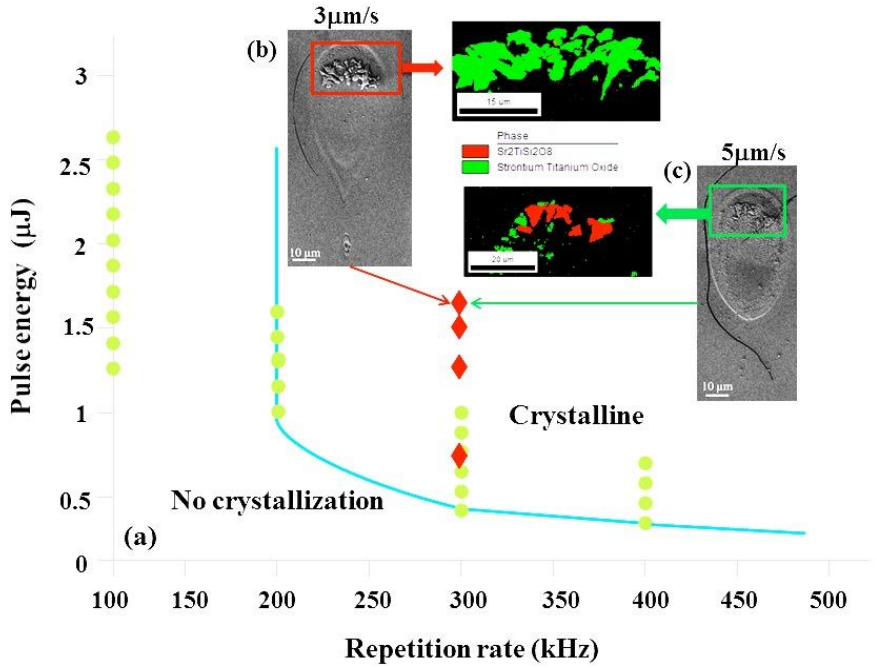

Fig. 1. (a) The different domains defined by pulse energy *vs.* repetition rate diagram in STS glass. SEM and EBSD images of written line cross sections irradiated at 1.7 µJ with a scanning speed at (b) 3 µm/s and (c) 5 µm/s, respectively are also shown. Green dots in the picture indicate the static irradiation; red rhombi indicate the scanning mode in this work.

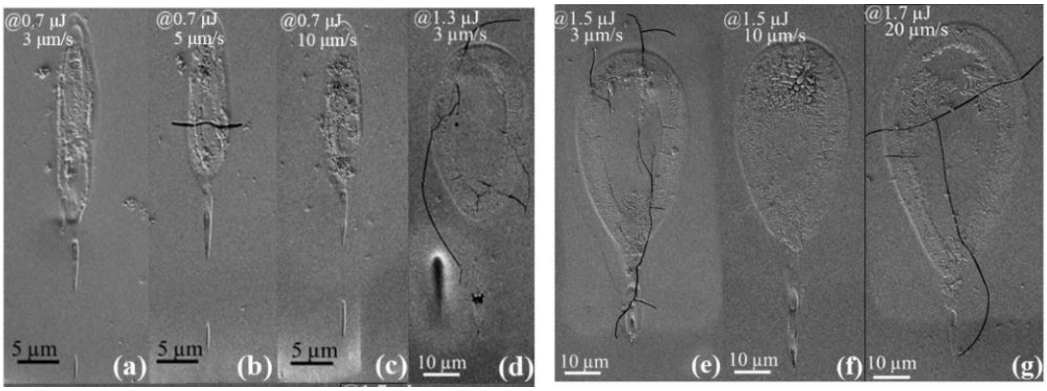

Fig. 2. SEM images of cross sections of written lines irradiated at 0.7 -1.7 µJ and 3-20 µm/s. At low energy, the HAV is completely rough because crystallized. At higher energy, a shell is rough; At further higher energy, the head is further crystallized.

Preprints (www.preprints.org) | NOT PEER-REVIEWED | Posted: 1 October 2020 doi:10.20944/preprints202010.0027.v1

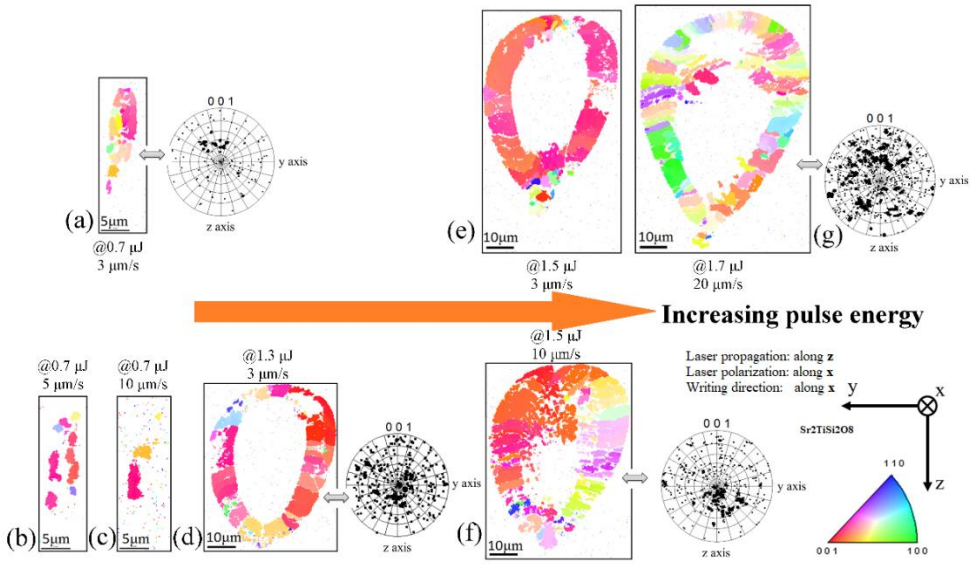

Fig. 3. EBSD inverse pole images of written line cross-sections irradiated at 0.7 -1.7 µJ and 3-20 µm/s writing velocity, coding the crystal orientation along x-axis. The pole figures give the angular distribution of the polar axis. The scanning direction and the laser polarization x are at the center of the pole figure.

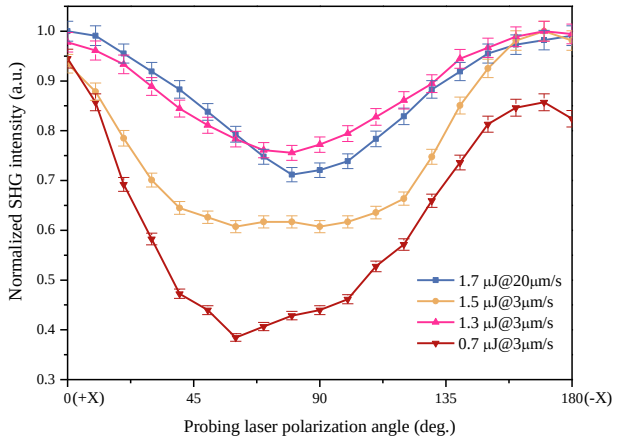

Fig. 4. Probe polarization angle dependence of SH intensity of the laser lines written at 0.7 µJ (red), 1.3 µJ (pink), 1.5 µJ (yellow), and 1.7 µJ (blue); the scanning direction is at 0°, Laser polarization is linear and parallel to x, the scanning direction.

Second Harmonic Generation (SHG) efficiency results of the texturation of non-linear polycrystals based on Fresnoite. The maximum of SHG is obtained when probing laser linear polarization is along the crystal polar axis. It is therefore a kind of measurement of crystal ordering that should be consistent with pole figure of the EBSD map. Fig. 4 shows the normalized SH intensity of crystal lines (irradiated at different pulse energies) as a function of probing laser polarization angle. The intensity maximum on all curves is around 0° excepted at the lowest energy for which a doubt can remain. The intensity minima are around 90° for the highest energy whereas for the smallest energy, the curve seems shifted in one direction. It is worth to note that SHG contrast defined by $(SHG_{max}-SHG_{min})/(SHG_{max}+SHG_{min})$, is the smallest at high energy whereas it is quite large for the smallest energy. It is about 42% at 0.7 µJ@3 µm/s, 12.9 % at 1.3 µJ@3 µm/s, 20 % at 1.5 µJ@3 µm/s, 16.8 % at 1.7 µJ@20 µm/s) indicating a weaker texturation at high energy.. It seems thus that are only one texture (polar c-axis in the direction of writing, mainly at low energy) and a large part of random orientation at higher pulse energy. This is quite different to what occurs in LNS glass for which there is two textures including one that is perpendicular to the direction of the polarization [27]. The angle shift we observe at low energy may be due to an effect of the Pulse Front tilt, an effect extensively described in [28]. In conclusion: low energy with low writing speed favored the formation of oriented crystals along the writing direction while increased pulse energy

Preprints (www.preprints.org) | NOT PEER-REVIEWED | Posted: 1 October 2020 doi:10.20944/preprints202010.0027.v1

at high writing speed mainly induced randomly oriented crystals. This is consistent with EBSD results shown in Fig. 3.

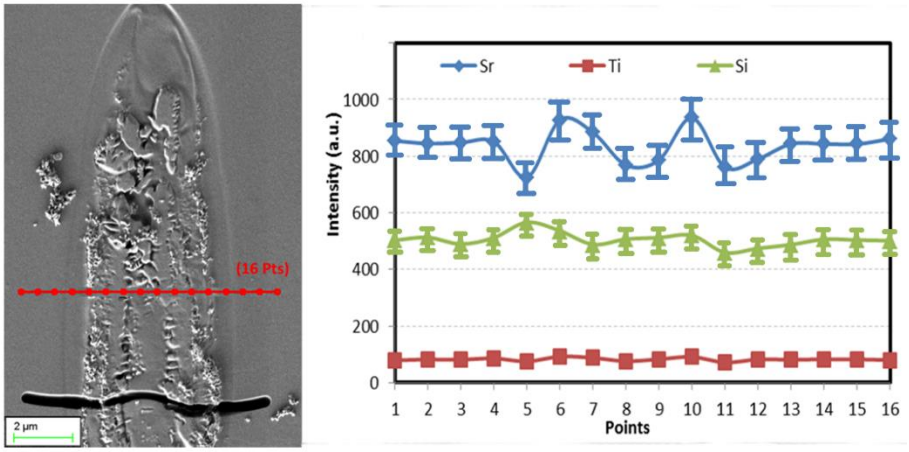

Fig. 5. SEM image and EDX line profile through a laser line cross section irradiated at 0.7 µJ and 5 µm/s. The measurement error is about 10%.

An elemental redistribution was also discovered after irradiation in STS glass, by energy-dispersive X-ray spectroscopy (EDX) as shown in Fig. 5. The relative compositional fluctuation for Sr element indicates a tendency to migrate towards the crystallized region whereas Si element preferred to concentrate in the amorphous zone at the center of the interaction volume. No apparent composition variation for Ti elements is detected. It has been published that thermal gradient determined the elemental migration tendency in glass [29-31]. In agreement with the literature, we observe that network formers (like Si element) concentrates at the center whereas the network modifiers, alkalin and earth alkaline (like Sr element) migrates out.

Discussion

First of all, we can be surprised to see that the lowest pulse energy for crystallization in LNS is close to the one for LNS glass (0.12-0.2W for STS and 0.16W for LNS glass) whereas the nucleation rate is known to be much faster for STS glass [8]. So, it seems that the nucleation rate is not the limitation in the related crystallization process. We can already hypothesize that the temperature field and its temporal evolution are the main parameters in the process.

When a fs laser beam is tightly focused in glasses, the laser intensity is high enough to enable nonlinear photoionization that relaxes mostly by electron-phonon coupling creating some local heating The energy carries by the laser beam is thus delivered to the material at the focal volume, and potentially cumulates pulse after pulse. Then, the heat diffuses away from that volume and the temperature that was very high in the focal volume after a few 10's ps, decreases until the next pulse. If the period between two consecutive pulses is much larger than the diffusion time $\tau_D=\omega_0^2/4D_T$ (where ω_0 is the beam waist radius and D_T the thermal diffusivity), ca. larger than $6\tau_D$, there is no heat accumulation and the time at high temperature is too small for inducing any phase transformation. On the contrary, when the repetition rate is large enough, period of time between consecutive pulses may be smaller than the heat diffusion time resulting in a heat accumulation. In these conditions, the T distribution changes its spatial and temporal shape mainly by broadening for radius larger than a few ω_0 from the beam [32]. If we define an average temperature at a point $\vec{r}$ of the material $\bar{T}(\vec{r},t_n)$ where t_n is the time of the n^{th} pulse, by $\bar{T}(\vec{r},t_n)=\int_{period\,\tau}\frac{T(\vec{r},t_n,t')}{\tau}dt'$ where τ is the period of the pulse, it evolves until a stationary state [32-34]. The time for that is also of about $6\tau_D$. This yield a temperature distribution in space that appears to be a bell shaped

Preprints (www.preprints.org) | NOT PEER-REVIEWED | Posted: 1 October 2020 doi:10.20944/preprints202010.0027.v1

curve around the beam. At pulse repetition rate large enough (ca. >30MHz for STS glass), it approaches the T distribution for a CW laser. In that case, the maximum T is defined by $T_{max} = \frac{E.f}{2\sqrt{\pi}\kappa w_0}$ with E the pulse energy, f the pulse repetition rate, κ the thermal conductivity. On the other hand as a first approximation, the shape of the function is defined only by the absorption coefficient (here a multiphoton coefficient) [35]. The width is just defined by the beam width but its shape is affected by the order of the multiphoton process that is highly non-linear. At the opposite, the T distribution associated to one pulse is quite different: the maximum temperature is given by $T_{max} = \frac{E.f}{\rho\, C_p}\frac{\pi^{3/2}}{{w_0}^2}\alpha$ with ρ the mass density, C_p the heat capacity, α the absorption coefficient (here multiphoton). Opposite to the CW case, the shape of this curve in time is defined by the thermal diffusion coefficient [36] e.g. the width is proportional to D_T. Of course, when the repetition rate *f* is intermediate, the T distribution shape is also intermediate. Fortunately, whatever the repetition rate, the shape is not distorted with the scanning provided that the speed is much smaller than the heat diffusion speed that we can estimate from the characteristic time τ_D for the heat to diffuse out of the waist i.e. $4D_T/\omega_0$ (ca. a few m/s), which is our case as the effective scanning speed for crystallization is smaller than 100 µm/s.

So the average temperature space and time distributions can be controlled and use for space-selective crystallization, which was described in ref [16]. Considering a point in the material at some distance of the center of the T bell shape, it experiences an increase of T followed by a subsequent decrease controlled by the heat diffusion coefficient in our conditions that we call thermal treatment curve quoted TTC. If T and scanning speed are suitable, some phase transformations can occur. The volume of the material where this happens defines the heat-affected volume (HAV). There are several cases that depend on the amplitude of the TTC.

a) **When the pulse energy is quite low (a few 0.1 µJ) but above the threshold for observing crystallization,** T_{max} can be nevertheless lower than the melting temperature of the Fresnoite crystal i.e. 1312°C [37]. The TTC may then cross the crystallization domain as it is exemplified in Fig. 6(b) whereas Fig. 6(a) gives a classic definition about TTT (Temperature Time Transformation) and CCT (Continuous Cooling Transformation) curves. So the crystallization begins with homogeneous nucleation (the lowest side of the domain) and then goes on crystal growing (the highest side). This is achieved at any place of the HAV and may form a complete crystallized volume. Its size is comparable to the laser beam size as it is demonstrated in [16]. Note there is homogeneous nucleation but the growth of the nuclei is favored when their c-axis are oriented in the direction of scanning because c-axis exhibits the fastest growth rate in such a structure [38] and aligned with the largest gradient (like in the method of single crystal growth by floating zone).

When the scanning speed is increased, the growth of previously nucleated nanocrystals during the T increase has not enough time for growing. Crystals with other orientations appear therefore if there is no other driving force that can be involved. Here, with STS we do not observe another texture than the one cited above, but in LNS glass we pointed out an orientable texture controlled with the laser polarization [17]. These two distinct behaviors are likely due to the large difference in nucleation and growth speeds: a few µm/s in LNS and at least two order of magnitude higher for STS ([21], [22])

b) **When the pulse energy is increased, a part of the temperature distribution may overcome the melting temperature (i.e. T_m≈1350 °C) and a stable liquid phase appear**s. In such a case, the TTC part to take into account starts from T_m (see Fig. 6(c)). It is only decreasing (cooling curve) and then may cross the crystallization domain from the growth side (the top of the domain, in fact). The crystallization is thus non homogeneous and is very sensitive to interfaces with the peripheral part of the HAV that is already crystallized because it started sooner in the course of the scanning. In the case of LNS glass, the center

Preprints (www.preprints.org) | NOT PEER-REVIEWED | Posted: 1 October 2020 doi:10.20944/preprints202010.0027.v1

is thus filled in by crystal having the orientation of the surrounding crystallized region [39] [40]). However, here in STS glass, the elemental migration is effective and leads to a decrease of the Sr concentration in the center of the HAV and an increase of Si content which modify the crystallization temperature and time conditions. As we observed an amorphous state in this region, we have to conclude that this migration prevents the Fresnoite crystallization. *Therefore, we conclude the appearance of a crystallized shell marks the domain of homogeneous crystallization, so the domain with $T<T_m$ and the interior boundary is the surface with $T=T_m$.*

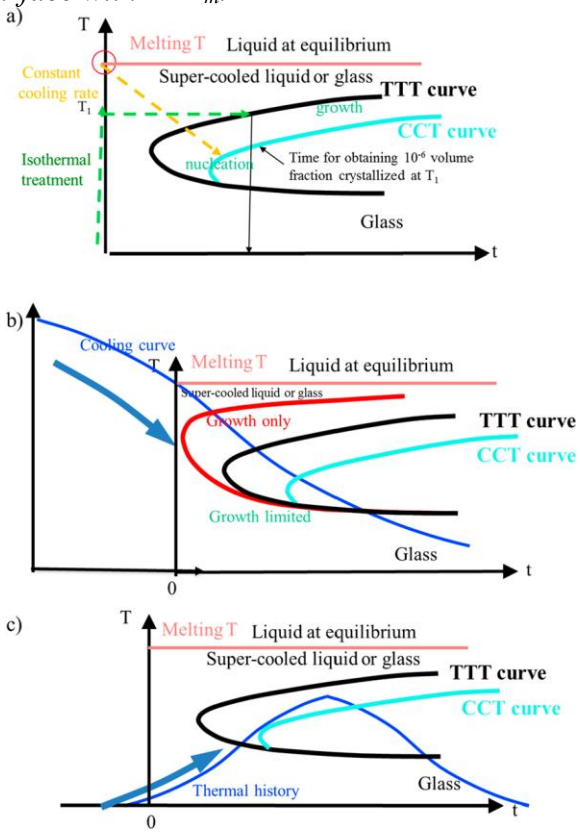

Fig. 6. (a) The Temperature Time Transformation (TTT) and Continuous Cooling Transformation (CCT) curves (CCT curve appears shifted from the TTT one a little to the downward right). This is because the lower growth rate is integrated during the cooling process from the melt to a given T. Thus, the time required for obtaining the same amount (e.g., 10^{-6}) is larger); (b) position of the TTC for places experiencing a TTC with a maximum average T larger than Tm. The red curve corresponds to growth rate only. It is applicable when nucleation sites already exist; (c) position of the TTC for places experiencing maximum temperature smaller than melting temperature (Fig.15 from ref [16]).

About the size of the heat affected volume: Now if we compare the size of the heat-affected volume between STS and LNS glasses (see Fig.7), we find that the width and the length of the HAV are much larger for STS glass. As a matter of fact, they are defined by the size of the bell shape temperature distribution that is itself defined by several glass properties: the thermal conductivity, the heat capacity, the specific density and thus the thermal diffusivity. The Table 1 compares their values.

Preprints (www.preprints.org) | NOT PEER-REVIEWED | Posted: 1 October 2020 doi:10.20944/preprints202010.0027.v1

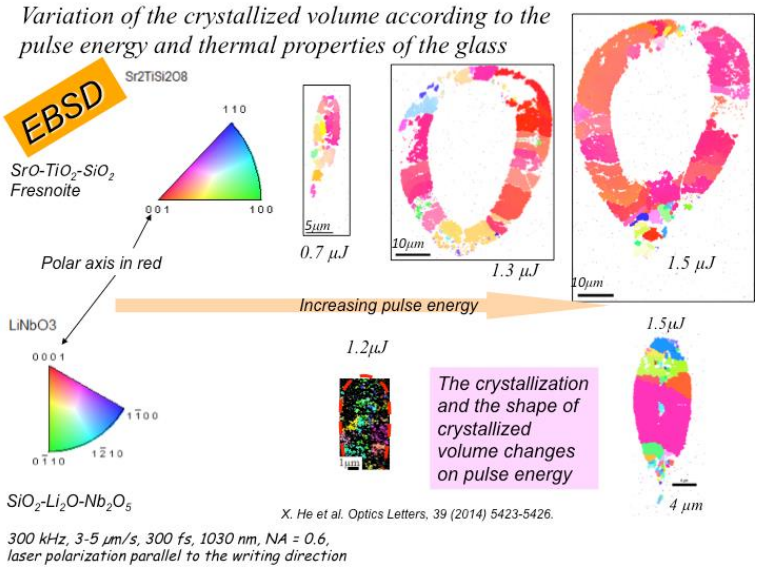

Fig.7. Comparison of the size of the heat affected volume in STS and LNS glass.

Table 1: Physico-chemical data for STS and LNS glasses

	STS glass	LNS glass	ref
Heat capacity Cp	*410 J.kg^{-1}.K^{-1}*	650 *J.kg^{-1}.K^{-1}*	[21] and [41]
Specific mass ρ	*3887 kg/m^3*	*3830 kg/m^3*	[42] and interpolation
Thermal conductivity κ	*10.1J/Kms*	2,65*J/Kms*	Deduced from diffusivity
Thermal diffusivity D_T	70×10^{-7} m^2/s	9×10^{-7} m^2/s	Interpolated from [43, 44]
Melting T_m (°C)	Sr-Fresnoite =1312	LiNbO3 =1257	[37] and [45]
Glass temp. T_g (°C)	760	551	[21] and [46]
Bandgap (eV)	5.1	3.7-4.7	[47] and [48]

However these physico-chemical quantities are involved differently in the T distribution as we say at the beginning of the discussion section. After a limited number of pulses corresponding to ca. 5.τ_D, the T distribution reaches a steady state that corresponds to the bell shape curve.

When the repetition rate is much smaller than 1/τ_D, the width of the T curve is defined by the thermal diffusivity. We note that the thermal diffusivity is 8 times larger in STS glass. The maximum T is defined by ρC_p and the size of the irradiated volume ($\pi w_0^2/\alpha$, see above) and we note that ρC_p is 1.56 times smaller for STS. About the irradiated volume, the focusing conditions mainly (with some material correction) define its width but since it does not change a lot from a glass to another, we can be concluded to be 3µm in our conditions. The length or the height of the HAV (in the direction of the laser propagation) is more difficult to estimate. For that purpose, we can consider that the heat diffusion is isotropic from the beam, either along or perpendicular to the laser propagation axis. The characteristic length of diffusion is thus roughly the same either from the waist or from the multiphoton absorption length 1/α, which are around 13µm for STS and 15µm for LNS. This is quite realistic as their optical bandgap are similar (see Table 1) and their multiphoton ionization coefficient probably also, as their electronic structure are similar (p orbitals of oxygen for the top of the valence band and d orbital of Ti or Nb for the bottom of the conduction band).

If the repetition rate f was high enough in such a way the steady state will approach the CW distribution, the HAV size would be just sensitive to α and we would expect the same size for both STS and LNS. In this case, as the T maximum is reversely proportional

Preprints (www.preprints.org) | NOT PEER-REVIEWED | Posted: 1 October 2020 doi:10.20944/preprints202010.0027.v1

to the thermal conductivity κ it would be 8 times smaller for STS than for LNS. This is clearly not the case,. In addition, $1/\tau_D$ is 28MHz for STS and 3.6MHz for LNS that should be compared to our repetition rate i.e. 300kHz. So, the T distribution at the steady state (after $6\tau_D$) for LNS is closer to CW regime but neither STS nor LNS are close enough to say that their width is not dependent on κ. On the other hand, as their absorption coefficients are close to each other, there is no difference in the width arising from this.

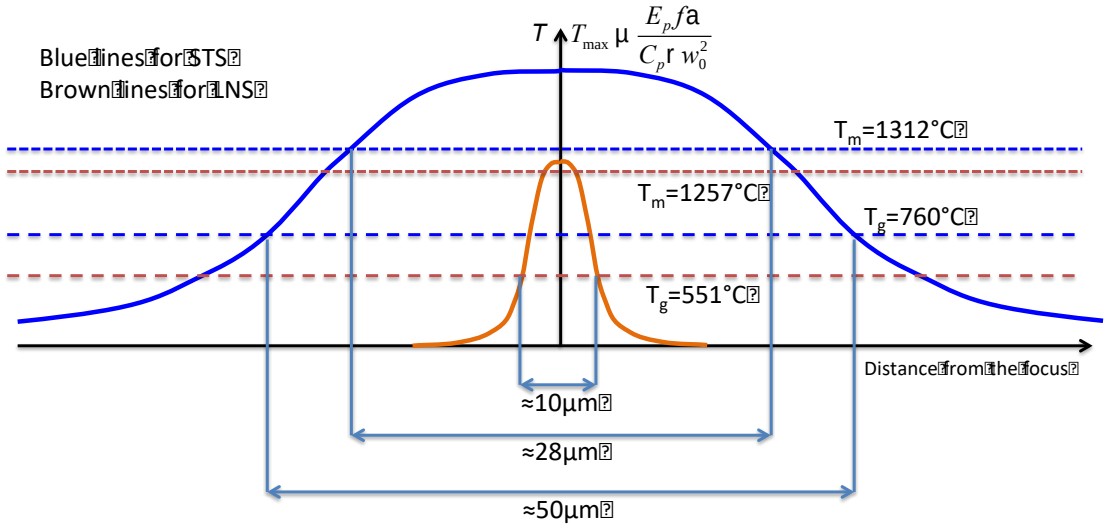

Fig. 8. Differences of the T distribution of STS and LNS glasses in the conditions of the fig.7. Sum-up of the discussion.

The conclusions are sum-up in Fig. 8. The maximum of T in the STS glass is higher than the one of the LNS glass due to $C_p\rho$ difference. The width of the T distribution of the STS glass is much larger due to diffusion coefficient difference. The the maximum of T for LNS is close to the melting T and the HAV is completely crystallized whereas for STS a large part of the HAV is above the melting T that cannot crystallize due to Sr/Si migration. So, crystallization occurs only in the volume shell between T_g and T_m.

Of interest it is worthy to note that the minimum energy E_m for TTC to touch the crystallization domain can be estimate by saying that the maximum T of this curve ($T_{max} = \frac{E.f}{\rho C_p}\frac{\pi^{3/2}}{w_0{}^2}\alpha$) should overcome T_g. So, E_m scales as $\rho C_p T_g/\alpha$, which is close to each other within 30%. We have also pointed out that for high pulse energy and low speed (e.g. 1.7 μJ, 3μm/s), a second phase appears ($SrTiO_3$). We think that this is the result of Sr out diffusion Therefore, varying the fs laser parameters, induced crystallization in STS glass can produce, a mixture of $SrTiO_3$ and $Sr_2TiSi_2O_8$ or pure $Sr_2TiSi_2O_8$ crystals by adjusting laser parameters. Similar results were reported by Y. Yonesaki et al. [49].

Lastly, we can add also that we have not found any spure of nanograting (a kind of organized submicrostructure pointed out in silica [50] by P. Kazansky) that one found in many compounds nowadays [51] and that we found in LNS glass [52]. We can hypothesize that the reason is the congruency of the glass in the case of STS.

4. Conclusion

In summary, systematic studies of laser-induced crystallization according to *pulse energy, repetition rate and scanning speed* have been achieved in STS glass ($2SrO\text{-}1TiO_2\text{-}2SiO_2$) and compared to results for LNS glass ($1Li_2O\text{-}1Nb_2O_5\text{-}1SiO_2$). Depending on these laser processing parameters, crystallization differs in size, morphology, texturation and also in phase composition i.e. distribution to the crystalline phases (both $SrTiO_3$ and $Sr_2TiSi_2O_8$ phases are precipitated for high energy and low speed). When only Fresnoite phase is detected in the heat-affected volume, this one is fully crystallized at low energy whereas an amorphous volume

remains surrounded by a crystallized shell at higher energy. This is quite different to what occurs for LNS glass. We demonstrate that both thermal conditions (due to the physic-chemical properties difference) and Sr/Si chemical migration under thermal gradient play important roles in this morphology. The crystallized shell is generally disordered but, for moderate speed (≈3μm/s), we observe the appearance of a texture where c-axis is aligned in the direction of scanning (this is observed frequently using CW or pulsed lasers and interpreted by the influence of the movement on the temperature gradient). This leads to the elaboration of a tube made of non-linear optical crystals having the largest SHG efficiency along the tube axis (it is also the same for pyro and piezo-electric properties). We believed that it would be an optical waveguide structure but as $Sr_2TiSi_2O_8$ (3.887 g/cm^{-3} [53] in STS glass (3.600 g/cm^{-3} [54]) has probably a larger refractive index that the inside of the tube, it is rather an anti-guiding structure. Otherwise, Fresnoite crystal is also polar but not ferro-electric and as the laser induced crystallization is like the drawing in floating zone method, the tube is probably not a waveguide but nevertheless an interesting structure for fabricating integrated nonlinear optical devices.

Lastly, at this stage of the study, we have not found a domain of oriented nanocrystallization controlled by the laser polarization, as we reported for LNS glass. If such a domain exists, it would be located between 0.3 and 0.7μJ at 300 kHz for scanning speed high enough. Just above the crystallization threshold, there is nanocrystallization in LNS glass filling partially the HAV whereas in STS the HAV is fully crystallized. This arises likely from the nucleation speed difference between the two families (a few μm/s in LNS whereas it is at least two orders of magnitude higher in STS[21]). The growth rates are also with the same trend[22]. Therefore, the effect of laser polarization acting on nanocrystals was not pointed out in STS glass.

Acknowledgements

This research work was financially supported by the National Natural Science Foundation of China (51572202, 61604110) and Shenzhen basic research (JCYJ20150417142356651). It was achieved in the frame of FLAG (Femtosecond Laser Application in Glasses) consortium project with the support of the Agence Nationale pour la Recherche (ANR-09-BLAN-0172-01) and the French Foreign Office (Eiffel program).

Author contributions: Conceptualization, X. He, B. Poumellec; Methodology, B. Poumellec; Investigation, X. He and F. Brisset; Original draft preparation and Writing, X. He, B. Poumellec; Review and editing, Project administration, B. Poumellec and M. Lancry; Supervision and Funding acquisition, Q. Liu and B. Poumellec

Conflicts of interest: none.

References

1. Choi, J., et al., *Three-dimensional direct femtosecond laser writing of second-order nonlinearities in glass.* Optics Letters, 2012. **37**(6): p. 1029-1031.
2. Liu, Q.M., et al., *Second-harmonic generation in Ge20As25S55 glass irradiated by an electron beam.* Optics Letters, 2001. **26**(17): p. 1347-1349.
3. Takahashi, Y., et al., *Optical Second Order Nonlinearity of Transparent Ba2TiGe2O8 Crystallized Glasses.* Applied Physics Letters, 2002. **81**(2).
4. Ochi, Y., T. Meguro, and K. Kakegawa, *Orientated crystallization of fresnoite glass-ceramics by using a thermal gradient.* Journal of the European Ceramic Society, 2006. **26**(4-5): p. 627-630.
5. Ding, Y., et al., *Preparation of polar oriented Sr2TiSi2O8 films by surface crystallization of glass and second harmonic generation.* Journal of Non-Crystalline Solids, 1996. **203**: p. 88-95.

6. Oikawa, T., T. Honma, and T. Komatsu, *Laser‐induced crystal growth of nonlinear optical Ba3Ti3O6(BO3)2 on glass surface.* Crystal Research & Technology, 2008. **43**(12): p. 1253-1257.
7. Komatsu, T. and T. Honma, *Nucleation and Crystal Growth in Laser-Patterned Lines in Glasses.* Frontiers in Materials, 2016. **3**(32).
8. Komatsu, T., *Design and control of crystallization in oxide glasses.* Journal of Non-Crystalline Solids, 2015. **428**: p. 156-175.
9. Miura, K., et al., *Space-selective growth of frequency-conversion crystals in glasses with ultrashort infrared laser pulses.* Optics Letters, 2000. **25**(6): p. 408-410.
10. Dai, Y., et al., *Direct writing three-dimensional Ba2TiSi2O8 crystalline pattern in glass with ultrashort pulse laser.* Applied Physics Letters, 2007. **90**(18): p. 181109.
11. Stone, A., et al., *Direct Laser-Writing of Ferroelectric Single-Crystal Waveguide Architectures in Glass for 3D Integrated Optics.* Scientific Reports, 2015. **5**: p. 10391.
12. Svaasand, L.O., et al., *Solid-solution range of LiNbO3.* Journal of Crystal Growth, 1974. **22**(3): p. 230-232.
13. Cao, J., et al., *Modifications in lithium niobium silicate glass by femtosecond laser direct writing: morphology, crystallization, and nanostructure.* Journal of the Optical Society of America B, 2017. **34**(1): p. 160-168.
14. Fan, C., *Contribution to nano or micro crystallization induction in silica-based glass by femtosecond laser irradiation*. 2012: Paris 11.
15. Musgraves, J.D., K. Richardson, and H. Jain, *Laser-induced structural modification, its mechanisms, and applications in glassy optical materials.* Optical Materials Express, 2011
. **1**(5): p. 921-935.
16. Cao, J., et al., *Femtosecond Laser-Induced Crystallization in Glasses: Growth Dynamics for Orientable Nanostructure and Nanocrystallization.* Crystal Growth & Design, 2019. **19**(4): p. 2189-2205.
17. Cao, J., et al., *Tunable angular-dependent second-harmonic generation in glass by controlling femtosecond laser polarization.* Journal of the Optical Society of America B, 2016. **33**(4): p. 741-747.
18. Wisniewski, W., K. Thieme, and C. Russel, *Fresnoite glass-ceramics - A review.* Progress in Materials Science, 2018. **98**: p. 68-107.
19. Lipat'ev, A.S., et al., *Femtosecond Laser Assisted Local Crystallization of Barium-Titanate-Silicate Glass.* Glass and Ceramics, 2018. **74**(11-12): p. 423-427.
20. Höche, T., C. Rüssel, and W. Neumann, *Incommensurate modulations in Ba_2TiSi_2O8, $Sr_2TiSi_2O_8$, and $Ba_2TiGe_2O_8$.* Journal of Solid State Chemistry, 2002. **166**(1): p. 15-23.
21. Wisniewski, W., K. Thieme, and C. Rüssel, *Fresnoite glass-ceramics – A review.* Progress in Materials Science, 2018. **98**: p. 68-107.
22. Fokin, V.M., M.L.F. Nascimento, and E.D. Zanotto, *Correlation between maximum crystal growth rate and glass transition temperature of silicate glasses.* Journal of Non-Crystalline Solids, 2005. **351**(10): p. 789-794.
23. Dai, Y., et al., *Space-selective precipitation of functional crystals in glass by using a high repetition rate femtosecond laser.* Chemical Physics Letters, 2007. **443**(4-6): p. 253-257.
24. He, X., et al., *One-step photoinscription of asymmetrically oriented fresnoite-type crystals in glass by ultrafast laser.* Optics Letters, 2014. **39**(18): p. 5423-5426.
25. He, X., et al., *Size-controlled oriented crystallization in SiO₂-based glasses by femtosecond laser irradiation.* Journal of the Optical Society of America B, 2014. **31**: p. 376-381.
26. Poumellec, B., et al., *Modification thresholds in femtosecond laser processing of pure silica: review of dependencies on laser parameters [Invited].* Optical Materials Express, 2011. **1**(4): p. 766-782.
27. Cao, J., et al., *Angular Dependence of the Second Harmonic Generation Induced by Femtosecond Laser Irradiation in Silica-Based Glasses: Variation with Writing Speed and Pulse Energy.* World Journal of Nano Science and Engineering, 2015. **Vol.05No.03**: p. 11.
28. Poumellec, B., et al., *Asymmetric Orientational Writing in glass with femtosecond laser irradiation.* Optical Materials Express, 2013. **3**: p. 1586-1599.
29. Zhang, F., et al., *Femtosecond laser induced migration of alkali ions in calcium silicate glasses.* Materials Letters, 2014. **137**: p. 92-95.
30. He, X., et al., *One-step photoinscription of asymmetrically oriented fresnoite-type crystals in glass by ultrafast laser.* Optics Letters. **39**(18): p. 5423.
31. Shimizu, M., et al., *Formation Mechanism of Element Distribution in Glass Under Femtosecond Laser Irradiation.* Optics Letters, 2011. **36**(11): p. 2161-2163.
32. Vogel, A., et al., *Mechanisms of femtosecond laser nanosurgery of cells and tissues.* Applied Physics B, 2005. **81**(8): p. 1015-1047.

33. Sanders, D.J., *Temperature distributions produced by scanning Gaussian laser beams.* Applied Optics, 1984. **23**(1): p. 30-35.
34. Miyamoto, I., et al., *Fusion Welding of Glass Using Femtosecond Laser Pulses with High-repetition Rates.* Journal of Laser Micro Nanoengineering, 2007. **2**(1): p. 57-63.
35. Lax, M., *Temperature rise induced by a laser beam.* Journal of Applied Physics, 1977. **48**(9): p. 3919-3924.
36. Miyamoto, I., A. Horn, and J. Gottmann, *Local Melting of Glass Material and Its Application to Direct Fusion Welding by Ps-laser Pulses.* Journal of Laser Micro Nanoengineering, 2007. **2**(1): p. 7-14.
37. Avramov, I., R. Keding, and C. Rüssel, *Crystallization kinetics and rigidity percolation in glass-forming melts.* Journal of Non-Crystalline Solids, 2000. **272**(2): p. 147-153.
38. Wisniewski, W., M. Patschger, and C. Russel, *Sr-fresnoite surface crystallisation in a 2SrO center dot TiO2 center dot 2.75 SiO2 glass studied by EBSD.* Crystengcomm, 2012. **14**(17): p. 5425-5433.
39. Cao, J., et al., *Pulse energy dependence of refractive index change in lithium niobium silicate glass during femtosecond laser direct writing.* Optics Express, 2018. **26**(6): p. 7460-7474.
40. Stone, A., et al., *Femtosecond laser-writing of 3D crystal architecture in glass: Growth dynamics and morphological control.* Materials & Design, 2018. **146**: p. 228-238.
41. *Chemical Engineering Catalog* Vol. Twelfth Annual Edition. 1927: The Chemical Catalog Company, Inc.
42. Fang, Z., et al., *Glass-ceramic optical fiber containing Ba2TiSi2O8 nanocrystals for frequency conversion of lasers.* Scientific Reports, 2017. **7**: p. 44456.
43. Kingery, W.D., *Thermal Conductivity: XII, Temperature Dependence of Conductivity for Single-Phase Ceramics.* Journal of the American Ceramic Society, 1955. **38**(7): p. 251-255.
44. Morgan, R.A., et al., *Measurement of the thermal diffusivity of nonlinear anisotropic crystals using optical interferometry.* Applied Optics, 1987. **26**(24): p. 5266-5271.
45. Vigouroux, H., *Etude de vitrocéramiques optiques pour le doublement de fréquence* 2012. p. 278.
46. Shimada, M., T. Honma, and T. Komatsu, *Laser patterning of oriented LiNbO3 crystal particle arrays in NiO-doped lithium niobium silicate glasses.* International Journal of Applied Glass Science, 2018. **9**(4): p. 518-529.
47. Li, Y., et al., *Electronic Structures and Pr3+ Photoluminescence Characteristics in Fresnoite, Sr-Frenoite, and Ge-Frenoite.* Journal of the American Ceramic Society, 2011. **94**(2): p. 496-500.
48. Thierfelder, C., et al., *Do we know the band gap of lithium niobate?* physica status solidi (c), 2010. **7**: p. 362-365.
49. Yonesaki, Y., et al., *Space-selective precipitation of non-linear optical crystals inside silicate glasses using near-infrared femtosecond laser.* Journal of Non-Crystalline Solids, 2005. **351**(10): p. 885-892.
50. Shimotsuma, Y., et al., *Self-organized nanogratings in glass irradiated by ultrashort light pulses.* Physical Review Letters, 2003. **91**(24): p. 247405.
51. Shimotsuma, Y., M. Sakakura, and K. Miura, *Photoinduced self-assembly of nanostructure*, in *77th JSAP Autumn Meeting*. 2016, Japan Society of Applied Physics: Niigata city, Niigata Prefecture. p. 13p-C301-7.
52. Cao, J., et al., *Nanoscale Phase Separation in Lithium Niobium Silicate Glass by Femtosecond Laser Irradiation.* Journal of the American Ceramic Society, 2017. **100**(1): p. 115-124.
53. Höche, T., et al., *The Crystal Structure of $Sr_2TiSi_2O_8$.* Journal of Solid State Chemistry, 2002. **166**(1): p. 15-23.
54. Halliyal, A., et al., *Grain-Oriented Glass-Ceramics for Piezoelectric Devices.* Journal of the American Ceramic Society 1984. **67**(5): p. 331-335.